Micro and Nanostructures 179 (2023) 207592

Contents lists available at ScienceDirect

Micro and Nanostructures

journal homepage: www.journals.elsevier.com/micro-and-nanostructures

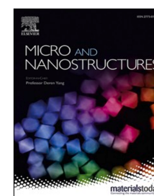

Optimization and fabrication of MEMS based piezoelectric acoustic sensor for wide frequency range and high SPL acoustic application

Ashish Kumar [a], Arathy Varghese [b,*], Girraj Sharma [c], Manish Kumar [d], Gaurav K Sharma [c], Mahanth Prasad [e], Vijay Janyani [c], R.P. Yadav [c], Khaled Elgaid [b]

[a] *Department of Electronics and Communication Engineering, National Institute of Technology, Raipur, 492010, India*
[b] *School of Engineering, Cardiff University, Cardiff, CF24 3AA, UK*
[c] *Department of Electronics and Communication Engineering, Malaviya National Institute of Technology, Jaipur, 302017, India*
[d] *Department of Electronics and Communication Engineering, GLA University, Mathura, 281406, India*
[e] *Transducers and Actuators Group, CSIR-Central Electronics Engineering Research Institute, Pilani, 333031, India*

ARTICLE INFO

Keywords:
Si-diaphragm
Microtunnel
FEM
LEM
Piezoelectricity
Acoustic sensor

ABSTRACT

This paper reports finite element model (FEM) simulation and fabrication of a square shaped diaphragm along with microtunnel for MEMS acoustic sensor which can be used for measurement of wide operational frequency range and high sound pressure level (SPL) 100 dB–180 dB measurement in launching vehicle and aircraft. The structure consists of a piezoelectric ZnO layer sandwiched between two aluminum electrodes on a thin silicon diaphragm. There is a microtunnel in the structure which relates the cavity to the atmosphere for pressure compensation. The microtunnel decides the lower cut-off frequency of device. Analytical and simulation approaches are used to optimize microtunnel dimension and simulation approach for diaphragm structure optimization. The change in displacement, stress, sensitivity and resonance frequency due to different diaphragm sizes with diaphragm thickness variation is also analyzed. The optimized diaphragm structure of 1750 × 1750 μm^2 and microtunnel of 100 μm wide and 24 μm deep have been fabricated using bulk micromachining technique. The fabricated device response has been tested using LDV and sensitivity measurement system.

1. Introduction

The increasing use of satellite and rocket launching vehicles, passenger and commercial aircraft become the cause of generating high sound pressure level (SPL) noise surrounding the airports and the launching pads. The generated sound has long term effects on humans and animals. The aircraft and launching vehicle manufacturers are insisted to reduce this noise in order to meet the quiet environment expectation by humans. Aeroacousticians these days make use of advanced techniques with noise reduction capabilities while designing aircraft and launching vehicles. Among these experimental techniques the major ones used recently include collection of distributed microphone arrays that can effectively measure sample spatial pressure fluctuations. Various configurations of microphone arrays have been deployed on the exterior of aircraft during flight tests to enable characterization of turbulent boundary layer.

* Corresponding author.
E-mail address: varghesea@cardiff.ac.uk (A. Varghese).

https://doi.org/10.1016/j.micrna.2023.207592
Received 6 February 2023; Received in revised form 18 March 2023; Accepted 11 April 2023
Available online 26 April 2023
2773-0123/© 2023 The Authors. Published by Elsevier Ltd. This is an open access article under the CC BY-NC-ND license (http://creativecommons.org/licenses/by-nc-nd/4.0/).

This can also help in identifying the noise sources or assessing the effectiveness of the noise reduction technologies used. The requirements for acoustic sensors or microphones used as measurement components are very demanding. The acoustic sensor should be compact size, passive, linear response at large sound pressure, broader bandwidth, robust to moisture and exhibit stability to large variations in temperature and humidity.

Microelectromechanical systems (MEMS) based acoustic sensor show promise for meeting the stringent performance needs for these applications at reduced cost, made possible using batch fabrication technology. MEMS devices which interconnect electrical and mechanical components at miniature scale, have become very popular in micromachining and manufacturing industry. The working of these devices depends upon used transduction mechanism such as mainly optical [1], capacitive [2–5] piezoresistive [6,7] and piezoelectric [8–10]. Among these transduction, piezoelectric offers some unique features like no input power supply required, linear response for wide dynamic range and low noise but it exhibits lower sensitivity [11,12]. Some researcher tried to enhance sensitivity by reducing tensile residual of the transducer structure using fully clamped [13], cantilever [14,15], diaphragm (square [16–18] and circular [19,20]) structures. Three free up edges of cantilever improve deflection greatly which reduces residual stress and increases sensitivity of the structure. However, cantilever based devices have lower reliability and operational frequency [17] which can be improved by diaphragm structures.

Generally, two types of diaphragm structure namely square [16–18] and circular [19,20] structure have been reported. The circular shaped diaphragm devices have higher sensitivity due to its uniform distribution of the stress along its circumference. The etching process of circular diaphragm is limited to isotropic etch property of dry etching such as deep reactive ion etching (DRIE) which requires proper control on process parameters and very high cost as compared to wet etching [21]. To reduce the cost and fabrication complexity, square shaped diaphragm based devices are widely being used in development of acoustic sensors [22–24], pressure sensor [7,25,26], ultrasonic transducers [27,28], tactile sensors [29], energy harvester [15,30,31] and etc.

Therefore, piezoelectric based MEMS acoustic sensor with square shaped diaphragm is a suitable candidate which can be used for high SPL (100–180 dB) measurement and source localization specially in aircraft and satellite launching vehicle. The high cost and process overheads involved necessitate the development of simulation models for sensor design optimization [32]. In this work, finite element method (FEM) and lumped element model (LEM) simulations have been used hand in hand to optimize the device design prior to the fabrication. The dimensions of diaphragm affect sensor parameters in term of stress, resonant frequency, sensitivity, operation frequency range and etc. The optimized structure is fabricated using bulk-micromachining and simulation solution of structure has validated with experimental results. The organization of the paper is as follows: section 2, discusses the modeling and simulation of the device structure. In section 3, fabrication process flow and development of structure have been reported. Conclusion has been presented in section 4.

2. FEM and LEM simulations

The proposed design consists of different layer like substrate (Si), insulator and passivation (SiO_2), top and bottom electrodes (Al) and piezoelectric (ZnO). This piezoelectric material is sandwiched between bottom and top electrodes. Fig. 1 shows cross-sectional view and back side view of the proposed structure. To optimize the design we have used FEM based MEMS tool CoventorWare 10.2. Material properties of the different layers have been taken as defined in CoventorWare database. The thickness of the thermal oxidation, insulator and passivation layer, top and bottom electrodes and piezoelectric material have been taken as 0.5 μm, 0.2 μm, 1 μm and 2 μm respectively. Different side lengths (1500 × 1500 μm^2, 1750 × 1750 $\mu m^2$and 2000 × 2000 μm^2) which chosen after considering available literature [19,24] with minimization of device dimensions and diaphragm thickness (15 μm, 20 μm and 25 μm) have been taken and comparison has been made. Fine meshing and 400Pa uniform load at top surface of the proposed design have been applied to get the simulation results.

Among these diaphragm sizes, the simulation results of 1750 × 1750 μm^2 with different thickness, 15 μm, 20 μm and 25 μm have been shown for reference and obtained simulation results with different diaphragm size and diaphragm thickness are summarized in Table 1. The distribution of deflection and stress in meshed structure have been shown in Figs. 2 and 3 respectively. From Table 1, it is

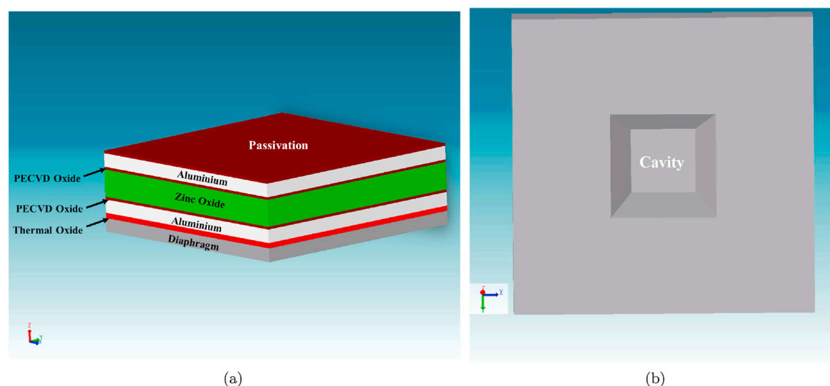

Fig. 1. Designed structure of acoustic sensor using MEMS tool CoventorWare: (a) cross sectional view and (b) back side.

inferred that deflection and generated stress increase with increase in area of diaphragm but they decrease with increase in thickness of diaphragm. Fig. 4 shows that the change in resonance due to change in diaphragm area and thickness. The resonant frequency decreases as diaphragm area increases while it increases with increase in the diaphragm thickness as shown in Table 1. Basically selection of diaphragm dimensions affects displacement, stress, dynamic range and operational frequency. Therefore, other parameter variation with diaphragm size should be analyzed.

2.1. Linear dynamic range

Linearity of any diaphragm based device is an important aspect when input pressure is large. Response of any mechanical sensing system can be approximately linear for small values of input pressure but at higher input pressure it deviate from actual value due to geometric non-linearity of the diaphragm. The linear dynamic range estimation for high SPL of the proposed diaphragm sizes has been done using simulation results as reported Kumar et al. (2019) [9]. These results show that the diaphragm size of 1750 × 1750 μm^2 has dynamic range of 100–180 dB which follows proposed deflection-linearity one fourth scaling model [33]. The proposed dynamic range is very utilitarian in pressure measurement of aircraft design and launching vehicles [34].

2.2. Operational frequency range

The LEM technique is used for the efficient analysis of the electrical behaviour of multiphysics systems like as electro-acoustic transducers [35]. In LEM, both the electrical and mechanical circuit analogies are used to evaluate the value of various lumped components such as diaphragm mass and compliance, cavity mass and compliance. The mathematical expression for these parameters are used as explained in Refs. [36,37]. These lumped element values have been calculated and simulated for the diaphragm size of 1750 × 1750 μm^2 and different thicknesses (15 μm, 20 μm and 25 μm) using NI Multisim and Ultiboard Education student Edition software. The simulated schematic of diaphragm 1750 × 1750 $\mu m^2$with 20 μm and the obtained bode plot have been shown in Fig. 5. The simulated results have been summarized in Table 2. From Table 2, it can be observed that flat response and resonant frequency increases with increment in thickness of diaphragm. It is demonstrated in previous works that linear response of the device can be observed if resonant frequency is higher than four times the operating frequency range of the device [38]. Therefore, the diaphragm thickness 20 μm has shown resonant frequency at 84 kHz which is approximately four times to bandwidth of audio frequency range. Based on the simulation results obtained for resonant frequency, dynamic range and operational frequency range analysis, It is observed that diaphragm size of 1750 × 1750 μm^2 with thickness 20 μm showed good response dynamic range of 100–180 dB, wide bandwidth 12 Hz-22kHz with 84 kHz resonant frequency. This dynamic range, resonant frequency and operational frequency range have capabilities to fulfil the requirement of measurement tools for pressure generated during launching satellite vehicle and aircraft application.

3. Modeling of microtunnel

The microtunnel structure has been modelled using electrical equivalent lumped element model (LEM). The proposed microtunnel has rectangular shape and its width (w = 100 μm) and depth (d = 24 μm) which assumed laminar tube with full flow of air in tube. The acoustic vent resistance (R) through microtunnel is defined as follows [39]:

$$R = \frac{128\mu_{air}L_{eff}}{\pi D_{vent}^4} \tag{1}$$

here μ_{air}, D_{vent} and L_{eff} represent viscosity of air, hydraulic diameter of microtunnel and effective microtunnel length. D_{vent} is defined as follows:

Table 1
Summary of the simulation results.

Diaphragm size [μm^2]	Thickness [μm]	Simulation parameters		
		Deflection [μm]	Stress [MPa]	Resonant freq. [kHz]
1500 × 1500	15	0.032	0.89	81.7
	20	0.016	0.54	112.6
	25	0.008	0.37	141.6
1750 × 1750	15	0.06	1.20	61.9
	20	0.029	0.73	82.7
	25	0.016	0.5	101.4
2000 × 2000	15	0.11	1.6	46.7
	20	0.049	0.96	63.3
	25	0.028	0.65	79.9

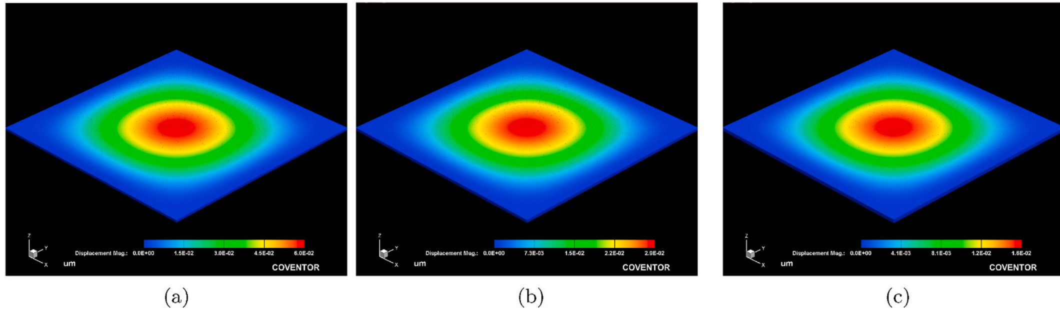

Fig. 2. Deflection distribution in diaphragm with thicknesses (a) 15 μm, (b) 20 μm and (c) 25 μm.

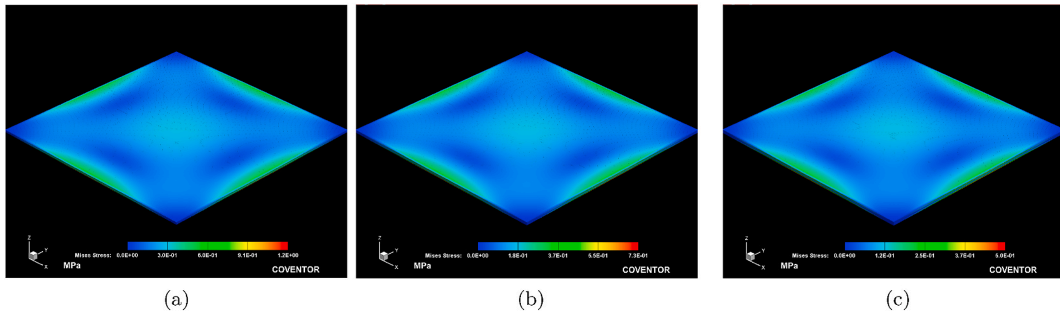

Fig. 3. Mises stress distribution in diaphragm with thicknesses (a) 15 μm, (b) 20 μm and (c) 25 μm.

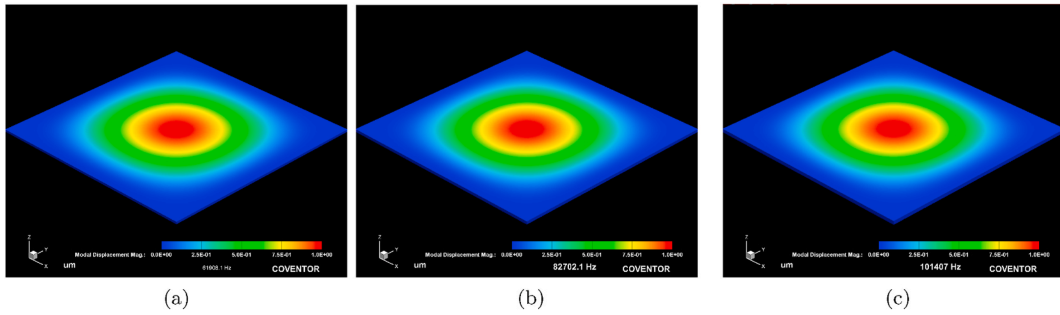

Fig. 4. Resonant frequency variation of diaphragm structure with thicknesses (a) 15 μm, (b) 20 μm and (c) 25 μm.

$$D_{vent} = \frac{2wd}{(w+d)} \tag{2}$$

The device lower cut off frequency can be evaluated as:

$$f_c = \frac{1}{2\pi R C_{cav}} \tag{3}$$

here C_{cav} stands for acoustic compliance of the cavity. An acoustic compliance is defined as follows:

$$C_{cav} = \frac{V_{cav}}{\rho_{air} c^2} \tag{4}$$

here V_{cav}, ρ_{air} and c stand for cavity volume, density of air and speed of sound. The dimensions of proposed design with diaphragm ($1750 \times 1750\ \mu m^2$) and other standard values have been taken and calculated $L_{eff} = 11833$ μm, $D_{vent} = 38.71 \times 10^{-6} m$, $R = 4 \times 10^{12} \Omega$, $V_{cav} = 1.47 \times 10^{-9} m^3$, and $C_{cav} = 1.036 \times 10^{-14} \frac{m^5}{N}$. By substituting the values of C_{cav} and R_a in Equation (15), the lower cut-off frequency was computed and found to be 4 Hz. The cut-off frequency of the designed structure is impacted by the width and depth of the microtunnel. The acoustic vent resistance is proportional to the inverse of the hydraulic diameter, which is determined by the

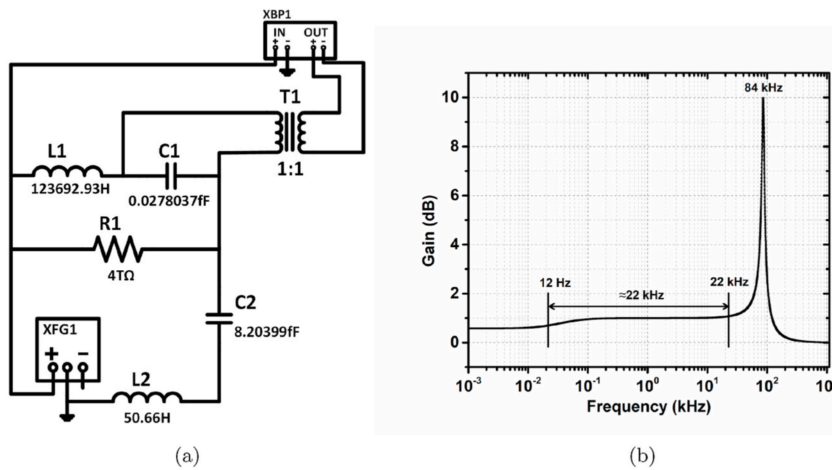

Fig. 5. LEM simulation results of 20 μm thick diaphragm: (a) equivalent schematic model and (b) bode plot.

Table 2
Summary of LEM results.

Diaphragm	Resonant freq.	Bandwidth	
thickness [μm]	[kHz]	[Hz]	[Hz]
15	64.1	11.4	26101
20	84.3	12.10	22652
25	104.6	15.602	18985

microtunnel's width and depth. Increasing these dimensions leads to a higher hydraulic diameter and a decrease in acoustic vent resistance, resulting in an increase in cut-off frequency. To achieve the lowest cut-off frequency with minimal fabrication complexity, the dimensions of the microtunnel have been optimized through simulations.

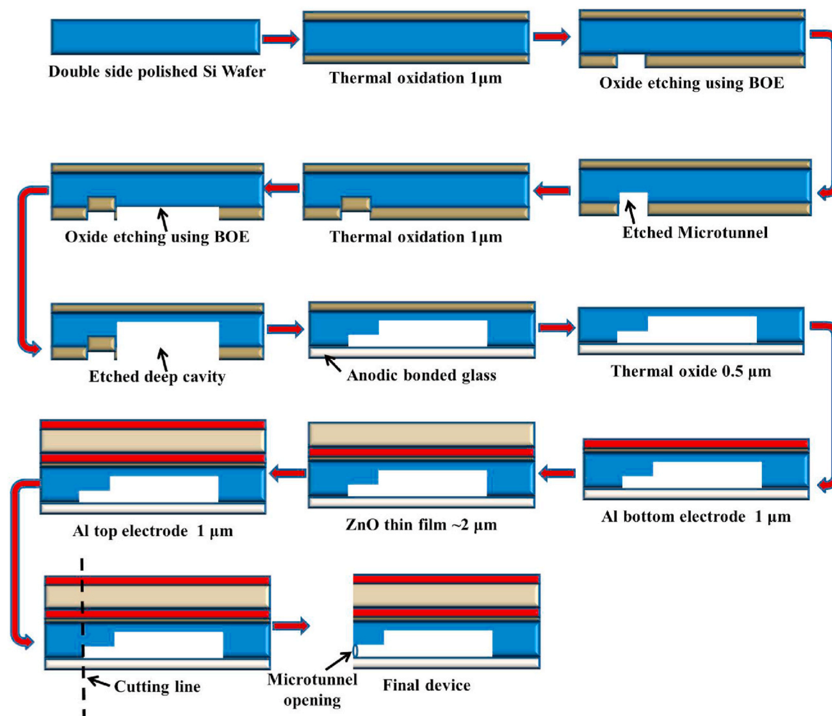

Fig. 6. Proposed fabrication process flow.

4. Fabrication and characterization

The analytical and simulation modelling of different diaphragm sizes can be concluded in terms of variation of deflection, stress, resonant frequency, operational frequency range and SPL range. This analysis helps to researchers for dimension selection of diaphragm based devices as interest of application requirement. The diaphragm dimension size of 1750 × 1750 μm^2 has been chosen to fabricate according to requirement MEMS based acoustic sensor for high SPL measurement. The proposed structure has operational frequency range (12 Hz-22kHz), SPL range (100dB–180dB), miniaturized device size and resonates approximately at 84 kHz which ensures flat response in audio and aeroacoustic frequency range. A piezoelectric transduction mechanism has been used for sensing duo to its unique features of linear response for wide dynamic range and zero input power requirement. Zinc oxide (ZnO) piezoelectric material is sandwiched between Aluminium (Al) top and bottom electrodes because it has well established deposition process and high piezoelectric coefficient. The deposition of ZnO and Al has been done at optimized conditions using RF-sputtering [12]. The fabrication process flow of the proposed structure has been shown in Fig. 6 and these steps have followed for fabrication. Fabrication process is started with selection of silicon wafer of 4 inch and it is cleaned with RCA-1 and 2 processes. Mask#1 is used to pattern the microtunnel area and etched with wet chemical processing. Mask#2 and SU-8 is used to pattern the diaphragm structure and the structure is etched using wet chemical etching process. Tetramethylammonium hydroxide (TMAH) etchant has been used for Silicon etching at 75° temperature environment. This wet etching process has been selected due to low cost and more selective process as compared to dry etching process. Fig. 7(a) shows an SEM image of backside of fabricated device which demonstrates formation of deep-cavity along-with microtunnel. Etched diaphragm structure is sealed with anodic glass and front side fabrication process is started with patterning of bottom Al electrode (Mask#3). The piezoelectric ZnO material is deposited using RF sputtering technique and patterned with help of Mask#4. From Fig. 8(a), it is clear that single peak at about 34.4° is present which is attributed to (002) preferred orientation of ZnO. Scanning electron microscopy has been used to ensure the structural morphology of the ZnO thin film as shown in Fig. 8(b). It is free from voids and clearly shows that the film is more uniformly deposited. Mask#5 is used to pattern the top Al electrode and etched with help of wet Al etchant solution. Mask#6 is used for pad opening. Fig. 7(b) depicts the front side SEM image of the fabricated device.

4.1. Wire bonding and packaging

A thin gold wire with a thickness of 17 μm is utilized to establish an electrical connection between the diced chip and a transistor outline header. This is done by fixing the diced chip onto the header with a curable epoxy, as shown in the optical image in Fig. 9. For device testing, ½″ stainless steel package has been designed and developed in which wire bonded TO header is placed for testing.

4.2. Resonant frequency response measurement

The diced chip has been fixed on the LDV measurement setup as shown in Fig. 10(a) to test resonant frequency and piezoelectric response. A 2 V electric potential has been applied on the fabricated device through device electrodes and probes. The deflection behaviour of the device diaphragm has been observed as showed in Fig. 10(b). It is observed that the fabricated device has maximum deflection on resonant frequency at 80 kHz. Resonant frequency of the clamped square diaphragm structure can be computed mathematically as given formula [40] by putting the value of diaphragm side length (2a = 1750 μm), diaphragm thickness (20 μm), density (2330 kg/m^3), Poisson's ratio (0.28) and Young's modulus (135 GPa) of silicon. The resonant frequency has been calculated and to be found 85.69 kHz. The measured resonant frequency of the fabricated device is lower than simulated and mathematically calculated values due to fabrication constraints.

4.3. Sensitivity measurement

The sensitivity measurement of the packaged device done as requires SPL sound generator and interfacing circuit to display the output voltage. Texas instruments integrated chip OPA129 operational amplifier as a charge amplifier and other components have been used to design interface circuit. B&K Sound Calibrator Type 4231 has been used as input sound pressure. Using interfacing circuit and sound calibrator, the sensitivity of the packaged device has been measured at 1 kHz frequency and is found to be 72 μV/Pa.

5. Conclusion

The FEM and LEM based simulation techniques have been used to optimize the dimensions of square shaped diaphragm and microtunnel. The diaphragm size 1750 × 1750 μm^2 with thickness 20 μm has been chosen to fulfill the need of wide operational frequency and high SPL in pressure measurement application of satellite launching vehicle and aircraft. The selected structures with optimized dimensions of diaphragm and microtunnel have been developed using bulk micromachining and standard complementary metal-oxide-semiconductor (CMOS) compatible processes on Si substrate. The fabricated piezoelectric (ZnO) device showed 80 kHz resonant frequency and 72 μV/Pa sensitivity. This analytical solution and proposed fabrication process flow for creation of smooth opening microtunnel in deep-cavity are very utilitarian in the development of acoustic sensor for high pressure measurement, chemical and biomedical applications.

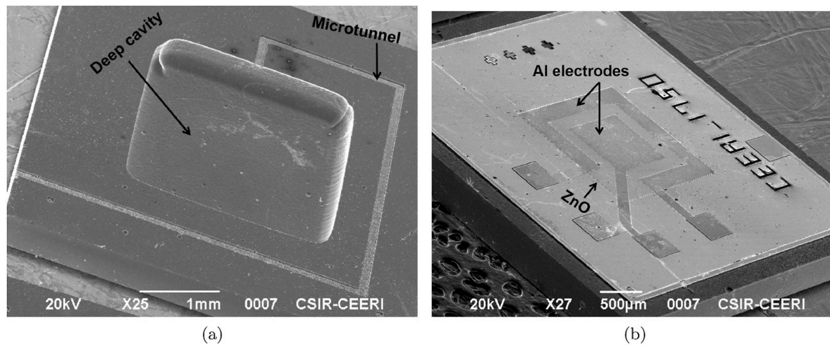

Fig. 7. SEM images of fabricated structure: (a) back side before anodic bonding and (b) front side.

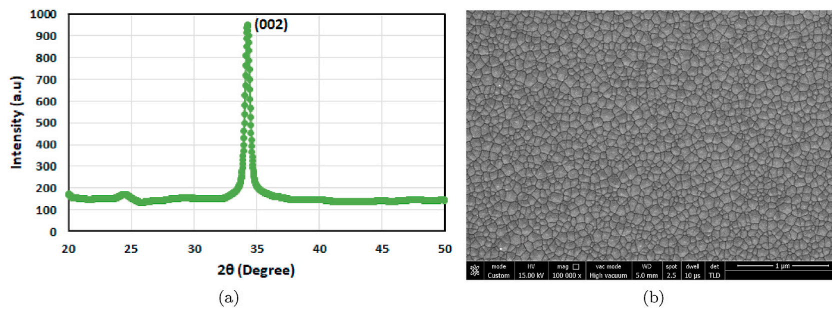

Fig. 8. ZnO thin film characterization (a) XRD spectra and (b) SEM image.

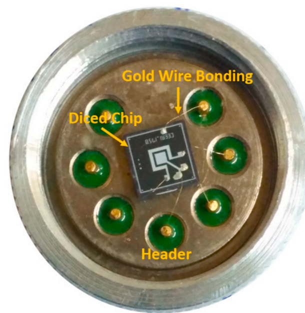

Fig. 9. Optical image of wire bonded chip.

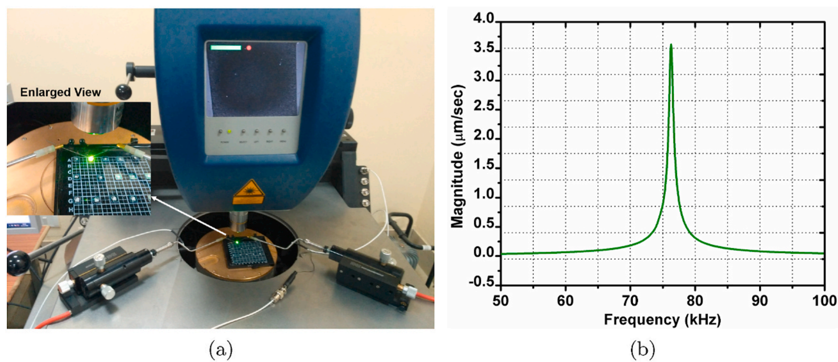

Fig. 10. Resonant frequency measurement (a) LDV setup with fixed device and (b) frequency response.

Author statement

Ashish Kumar: Conceptualization, Fabrication process development, Writing – review & editing, **Arathy Varghese**: Methodology, characterization, Investigation, Writing – original draft preparation, **Girraj Sharma**: Validation, Formal analysis, Writing – review & editing Author, **Manish Kumar**: Resources, Investigation, Writing – review & editing, **Gaurav K Sharma**: Methodology-frequency calculation, Writing – review & editing, **Mahanth Prasad**: Investigation, Resource, Writing – review & editing, **Vijay Janyani**: Ideation, Visualization, mentoring, Writing – review & editing, **R. P. Yadav**: Supervision, Writing – review & editing, Project administration. **Khaled Elgaid**: Supervision, fund support, Writing – review & editing, Project administration.

Declaration of competing interest

The authors declare that they have no known competing financial interests or personal relationships that could have appeared to influence the work reported in this paper.

Data availability

Data will be made available on request.

References

[1] Qiaoyun Wang, Qingxu Yu, Polymer diaphragm based sensitive fiber optic fabry-perot acoustic sensor, Chin. Opt Lett. 8 (3) (2010) 266–269.
[2] Altti Torkkeli, Outi Rusanen, Jaakko Saarilahti, Heikki Sepp, Hannu Sipola, Jarmo Hietanen, Capacitive microphone with low-stress polysilicon membrane and high-stress polysilicon backplate, Sensor Actuator Phys. 85 (1–3) (2000) 116–123.
[3] Michael Pedersen, Development of microelectromechanical systems capacitive microphone for high-frequency applications, J. Acoust. Soc. Am. 119 (5) (2006) 3378, 3378.
[4] Chun-Kai Chan, Wei-Cheng Lai, Mingching Wu, Ming-Yung Wang, Weileun Fang, Design and implementation of a capacitive-type microphone with rigid diaphragm and flexible spring using the two poly silicon micromachining processes, IEEE Sensor. J. 11 (10) (2011) 2365–2371.
[5] Michael L. Kuntzman, Gloria Lee Jia, Nishshanka N. Hewa-Kasakarage, Donghwan Kim, Neal A. Hall, Micromachined piezoelectric microphones with in-plane directivity, Appl. Phys. Lett. 102 (5) (2013).
[6] S. Santosh Kumar, B.D. Pant, Design principles and considerations for the 'ideal' silicon piezoresistive pressure sensor: a focused review, Microsyst. Technol. 20 (7) (may 2014) 1213–1247.
[7] S. Santosh Kumar, K Ojha Anuj, B.D. Pant, Experimental evaluation of sensitivity and non-linearity in polysilicon piezoresistive pressure sensors with different diaphragm sizes, Microsyst. Technol. 22 (1) (2016) 83–91.
[8] Shashikant Sharma, Sumit Vyas, C. Periasamy, P. Chakrabarti, Structural and optical characterization of zno thin films for optoelectronic device applications by rf sputtering technique, Superlattice. Microst. 75 (2014) 378–389.
[9] Ashish Kumar, Mahanth Prasad, Vijay Janyani, R.P. Yadav, Design, fabrication and reliability study of piezoelectric zno based structure for development of mems acoustic sensor, Microsyst. Technol. 25 (12) (2019) 4517–4528.
[10] Reza Ali Washim, Mahanth Prasad, Piezoelectric mems based acoustic sensors: a review, Sensor Actuator Phys. 301 (2020), 111756.
[11] Stephen Horowitz, Toshikazu Nishida, Louis Cattafesta, Mark Sheplak, Development of a micromachined piezoelectric microphone for aeroacoustics applications, J. Acoust. Soc. Am. 122 (6) (2007) 3428–3436.
[12] Ashish Kumar, Mahanth Prasad, Vijay Janyani, R.P. Yadav, Fabrication and annealing temperature optimization for a piezoelectric zno based mems acoustic sensor, J. Electron. Mater. (2019) 1–9.
[13] Seung S. Lee, Robert P. Ried, Richard M. White, Piezoelectric cantilever microphone and microspeaker, J. Microelectromech. Syst. 5 (4) (1996) 238–242.
[14] Xin Zhang, K.-S. Chen, R. Ghodssi, A.A. Ayon, S Mark Spearing, Residual stress and fracture in thick tetraethylorthosilicate (teos) and silane-based pecvd oxide films, Sensor Actuator Phys. 91 (3) (2001) 373–380.
[15] Shanky Saxena, Ritu Sharma, B.D. Pant, Fabrication and sensitivity analysis of guided beam piezoelectric energy harvester, IEEE Trans. Electron. Dev. 65 (11) (2018) 5123–5129.
[16] Choon Ko Sang, Yong Chul Kim, Seob Lee Seung, Seung Ho Choi, Sang Ryong Kim, Micromachined piezoelectric membrane acoustic device, Sensor Actuator Phys. 103 (1–2) (jan 2003) 130–134.
[17] Hong-Jin Zhao, Tian-Ling Ren, Jian-She Liu, Li-Tian Liu, Zhi-Jian Li, Fabrication of high-quality pzt-based piezoelectric microphone, in: TRANSDUCERS'03. 12th International Conference on Solid-State Sensors, Actuators and Microsystems. Digest of Technical Papers (Cat. No. 03TH8664), ume 1, IEEE, 2003, pp. 234–237.
[18] Reza Ali Washim, Mahanth Prasad, Design and fabrication of microtunnel and Si-diaphragm for ZnO based MEMS acoustic sensor for high SPL and low frequency application, Microsyst. Technol. 21 (6) (2015) 1249–1255.
[19] Seob Lee Woon, Seung S. Lee, Piezoelectric microphone built on circular diaphragm, Sensor Actuator Phys. 144 (2) (jun 2008) 367–373.
[20] Matthew D. Williams, Benjamin A. Griffin, Tiffany N. Reagan, James R. Underbrink, Mark Sheplak, An AlN MEMS piezoelectric microphone for aeroacoustic applications, J. Microelectromech. Syst. 21 (2) (apr 2012) 270–283.
[21] Ashish Kumar, Arathy Varghese, Anup Sharma, Mahanth Prasad, Vijay Janyani, R.P. Yadav, Khaled Elgaid, Recent development and futuristic applications of MEMS based piezoelectric microphones, Sensor Actuator Phys. 347 (nov 2022), 113887.
[22] B.A. Griffin, M.D. Williams, G. Wang, B.V. Sankar, L.N. Cattafesta, M. Sheplak, The electromechanical behavior of piezoelectric thin film composite diaphragms possessing in-plane stresses, J. Micromech. Microeng. 27 (4) (2017), 045017.
[23] Vasudha Hegde, Narendra Chaulagain, H.M. Ravikumar, Sonu Mishra, Siva Yellampalli, Modeling of microelectromechanical systems diaphragm based acoustic sensor, Int. J. Electr. Comput. Eng. 12 (2) (2018) 141–144.
[24] Mahanth Prasad, Vineet Sahula, Vinod Kumar Khanna, Design and fabrication of si-diaphragm, ZnO piezoelectric film-based MEMS acoustic sensor using SOI wafers, IEEE Trans. Semicond. Manuf. 26 (2) (may 2013) 233–241.
[25] Xiaodong Wang, Baoqing Li, Onofrio L. Russo, Harry T. Roman, K Chin Ken, Kenneth R. Farmer, Diaphragm design guidelines and an optical pressure sensor based on mems technique, Microelectron. J. 37 (1) (2006) 50–56.
[26] J. Dzuba, G. Vanko, M. Držík, I. Rỳger, V. Kutiš, J. Zehetner, T. Lalinskỳ, Algan/gan diaphragm-based pressure sensor with direct high performance piezoelectric transduction mechanism, Appl. Phys. Lett. 107 (12) (2015), 122102.
[27] E.S. Kim, Q.F. Zhou, J.M. Cannata, G.H. Feng, C. Sharp, K.K. Shung, Self-focused high frequency ultrasonic transducers based on ZnO piezoelectric films, Appl. Phys. Lett. 90 (11) (2007), 113502.
[28] Muralt Paul, Senior Member, Nicolas Ledermann, Jacek Baborowski, Abdolghaffar Barzegar, Sandrine Gentil, Brahim Belgacem, Sylvain Petitgrand, Alain Bosseboeuf, Setter Nava, Transducers based on PZT thin films, IEEE Trans. Ultrason. Ferroelectrics Freq. Control 52 (12) (2005) 2276–2288.

[29] Kentaro Nagamatsu, Narihito Okada, Hiroki Sugimura, Hirotoshi Tsuzuki, Fumiaki Mori, Kazuyoshi Iida, Akira Bando, Motoaki Iwaya, Satoshi Kamiyama, Hiroshi Amano, et al., High-efficiency algan-based uv light-emitting diode on laterally overgrown aln, J. Cryst. Growth 310 (7–9) (2008) 2326–2329.
[30] Huicong Liu, Jui Tay Cho, Chenggen Quan, Takeshi Kobayashi, Chengkuo Lee, Piezoelectric MEMS energy harvester for low-frequency vibrations with wideband operation range and steadily increased output power, J. Microelectromech. Syst. 20 (5) (2011) 1131–1142.
[31] Stephen B. Horowitz, Mark Sheplak, Louis N. Cattafesta III, Toshikazu Nishida, A mems acoustic energy harvester, J. Micromech. Microeng. 16 (9) (2006) S174.
[32] Ashish Kumar, Mahanth Prasad, Vijay Janyani, R.P. Yadav, Development of diaphragm and microtunnel structures for MEMS piezoelectric sensors, IEEE Trans. Semicond. Manuf. 33 (4) (nov 2020) 606–613.
[33] M.D. Giovanni, Flat and Corrugated Membrane Design Handbook, Mercel Dekker Inc, New York, 1982.
[34] Mehdi Khorrami, David Lockard, William Humphreys, Meelan Choudhari, Thomas Van de Ven, Preliminary analysis of acoustic measurements from the NASA-gulfstream airframe noise flight test, in: 14th AIAA/CEAS Aeroacoustics Conference (29th AIAA Aeroacoustics Conference), American Institute of Aeronautics and Astronautics, may 2008.
[35] Josef Merhaut, Theory of Electroacoustics, McGraw-Hill College, 1981.
[36] David Thomas Martin, of Ph.D. dissertation, Design, Fabrication, and Characterization of a MEMS Dual-Backplate Capacitive Microphone, ume 69, University of Florida, 2007.
[37] Dhairya Singh Arya, Sushil Kumar, Mahanth Prasad, Pushpapraj Singh, Chandra C. Tripathi, Design, modeling and simulation of square diaphragm based, piezoelectric (aln) mems acoustic sensor for high spl measurements, in: International Workshop on the Physics of Semiconductor and Devices, Springer, 2017, pp. 731–742.
[38] David T. Martin, Jian Liu, Karthik Kadirvel, Robert M. Fox, Mark Sheplak, Toshikazu Nishida, A micromachined dual-backplate capacitive microphone for aeroacoustic measurements, J. Microelectromech. Syst. 16 (6) (2007) 1289–1302.
[39] Philip J. Pritchard, John W. Mitchell, Fox and McDonald's Introduction to Fluid Mechanics, Binder Ready Version, John Wiley & Sons, 2016.
[40] P. Muralt, N. Ledermann, J. Paborowski, A. Barzegar, S. Gentil, B. Belgacem, S. Petitgrand, A. Bosseboeuf, N. Setter, Piezoelectric micromachined ultrasonic transducers based on PZT thin films, IEEE Trans. Ultrason. Ferroelectrics Freq. Control 52 (12) (2005) 2276–2288.